JOURNAL OF MATERIALS RESEARCH AND TECHNOLOGY 2022;18:4846–4858

Available online at www.sciencedirect.com

jmr&t Journal of Materials Research and Technology

journal homepage: www.elsevier.com/locate/jmrt

Original Article

Enhanced interfacial strength and ductility of stainless steel/carbon steel laminated composite by heterogenous lamella structure

Yaohua Yang [b,c], Zizheng Jiang [b,c], Xuefeng Liu [a,b,c,*], Jihong Sun [a,b,c], Wenjing Wang [b,c]

[a] Beijing Advanced Innovation Center for Materials Genome Engineering, University of Science and Technology Beijing, Beijing 100083, China

[b] Beijing Laboratory of Metallic Materials and Processing for Modern Transportation, University of Science and Technology Beijing, Beijing 100083, China

[c] Key Laboratory for Advanced Materials Processing of Ministry of Education, University of Science and Technology Beijing, Beijing 100083, China

ARTICLE INFO

Article history:
Received 26 February 2022
Accepted 11 April 2022
Available online 5 May 2022

Keywords:
Stainless steel/carbon steel laminated composite
Cladding interface
Heterogenous lamella structure
Interfacial shear strength
Ductility

ABSTRACT

Interfacial performance of stainless steel/carbon steel (SS/CS) laminated composite is crucial for further manufacturing and application. Here, we reported a new strategy for fabricating the SS/CS laminated composites that composed of heterogeneous lamella structure at the cladding interface zone, by employing liquid–solid bonding and subsequent hot rolling. Different rolling temperatures were applied for comparison of the formation of heterogeneous lamella structure and their influences on the mechanical properties of the cladding interface, and the mechanisms of enhanced interfacial shear strength and ductility by the heterogenous lamella structure were discussed. A metallurgical bonding interface with intensive elements diffusion was obtained by liquid–solid bonding method, and coarse equiaxed grains and a wider decarburized layer formed at the cladding interface zone. Under rolling temperature of 900 °C, the mechanical incompatibilities of cladding interface zone and lower temperature resulted in heterodeformation and inefficient driving force of recrystallization, resulting in a heterogenous lamella structure consisted of hardened austenite region, coarse-grained ferrite region and fine-grained pearlite and ferrite region at the cladding interface zone of SS/CS laminated composite, which obviously improved the interfacial shear strength and ductility of the SS/CS laminated composites due to back stress strengthening and hardening.

* Corresponding author.
E-mail address: liuxuefengbj@163.com (X. Liu).

https://doi.org/10.1016/j.jmrt.2022.04.057

1. Introduction

Stainless steel/carbon steel (SS/CS) laminated composites possess both excellent mechanical properties and low cost of CS and corrosion resistance of SS, which is a promising structural material for using in the field of chemical industry, petroleum and shipbuilding [1–4]. The performance of the cladding interface of the SS/CS laminated composites that connecting the SS and CS is crucial for the further manufacturing and application [5–8]. However, traditional bonding methods including explosion welding, diffusion bonding and hot rolling bonding result in limited diffusion distance of Cr, Ni and Fe elements through the cladding interface because of their lower diffusion coefficient under bonding conditions [9–12]. Additionally, remarkable diffusion of C element due to superior diffusion coefficient leads to the formation of decarburizing layer and carburizing layer at the cladding interface zone during bonding process, which significantly decreases the interfacial bonding strength of the SS/CS laminated composites [13–15]. As a consequence, the interfacial shear strength of the SS/CS laminated composites fabricated by vacuum diffusion bonding decreases with increasing bonding temperature or bonding time [10]. Apart from the diffusion, the stress and strain during hot rolling strongly affect the metal flow and microstructure evolution at the cladding interface zone, which also determines the interfacial bonding strength of the SS/CS laminated composites. Finer grains and oxides, decreased thickness of decarburizing and carburizing layers, increased diffusion distance of Fe, Cr and Ni elements are beneficial to improve the interfacial shear strength of the SS/CS laminated composites [12,15,16]. However, the differences between the diffusion coefficients of C, Fe, Cr and Ni elements restrict the improvement in the interfacial bonding strength of SS/CS laminated composites fabricated by solid–solid bonding method.

Heterostructured metals have recently attracted extensive interests in the materials community for their potential in achieving outstanding mechanical properties [17–20]. Wu et al. [18] reported that heterogeneous lamella-structured pure Ti possessed both the high strength of ultrafine grains and the decent ductility of the coarse grains. Ding et al. [21] proposed a new strategy for preparing heterostructured pure titanium laminates that possess a good combination of strength and ductility by combining gradient structure and heterogeneous lamella structure. Heterostructured metals contain interfaces, the adjacent regions of the interfaces are differences in chemical compositions and/or microstructures [22–24]. It was believed that the interfaces significantly contribute to the high strain hardening and ductility in heterostructured metals [25]. An interface-affected zone forms during deformation, and the non-uniform strain gradient and geometry necessary dislocations (GNDs) accumulation were generated via dislocation pile-up, inducing heterodeformation induced (HDI) strengthening and hardening within the interface-affected zone [19]. As a consequence, exploring a new preparation route to build the unique heterostructure within the cladding interface zone is a promising method for improving the mechanical properties of the SS/CS laminated composites.

The liquid–solid (L-S) bonding method is a promising technique for preparing laminate metal matrix composites due to its high efficiency, low cost and higher interfacial bonding strength. Currently, L-S bonding method has been widely used to prepare laminate metal matrix composites [26–28]. During L-S bonding process, the liquid metal wets and

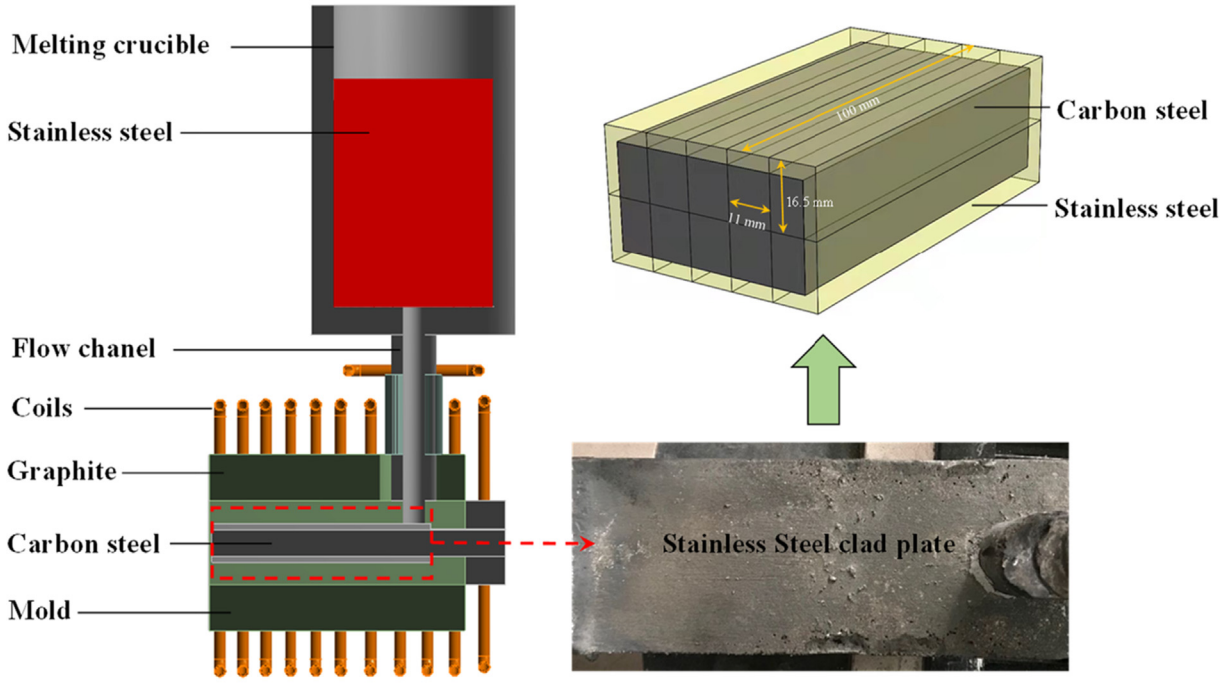

Fig. 1 – Schematic diagram of preparing SS/CS laminated composite by liquid–solid bonding method.

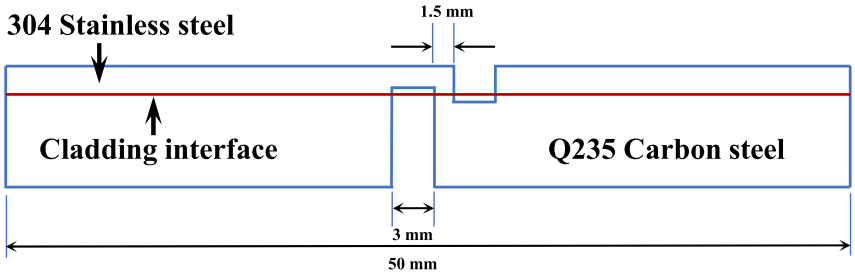

Fig. 2 – Dimensions of the tensile shear specimen.

spreads at the solid substrate at the beginning, and then intensive heat transfer occurs through the cladding interface. The temperature of the substrate sharply increases to the peak value and then decreases quickly, elements dissolution and diffusion at the cladding interface zone occur simultaneously [29–33]. Additionally, the melt inversely solidifies from the interface to the outside. The liquid–solid bonding process accelerates the elements diffusion at the cladding interface, which significantly improves the diffusion distance of alloy elements [34–36]. However, intensive heat transfer at the cladding interface zone always results in grain coarsening.

Hot working is a powerful tool to control the microstructures of polycrystalline metals. During hot working process of austenite, a large number of dislocations will pileup in the grain, promoting the nucleation and growth of dynamic recrystallization (DRX) crystal nuclei and constantly consuming the deformed tissue to achieve softening [37]. Carbon is an important alloying element in steel, and it will cause softening at a low strain rate while hardening at a high strain rate [38,39]. A larger initial grains size increases the deformation activation and reduces the number of grain boundaries acting as nucleation points, leading to the delay of DRX and an increase in flow stress, and greater strain is required for complete recrystallization [40–42]. Additionally, the deformation temperature and strain rate significantly affect the recrystallization kinetics and recrystallized grain size, and a Zener-Hollomon parameter incorporating deformation temperature and strain rate is usually used to study DRX [43–45]. The recrystallization kinetics and steady state grain size increase with increasing deformation temperature and decreasing strain rate [46].

Based on the discussion above, we proposed a new strategy for producing the SS/CS laminated composites that composed of heterogeneous lamella structure at the cladding interface zone, by employing L-S bonding and subsequent hot rolling (L&R). The aim is to achieve the novel heterogeneous interface zone with superior combination of high strength and ductility of the cladding interface. Different rolling temperatures were applied

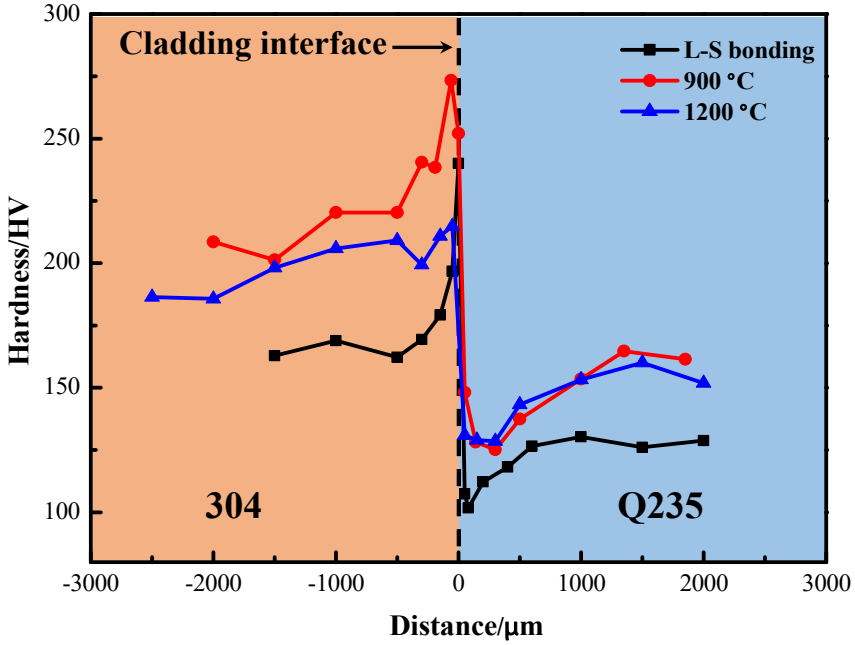

Fig. 3 – Variation of microhardness across the cladding interface of SS/CS laminated composites with different processing parameters.

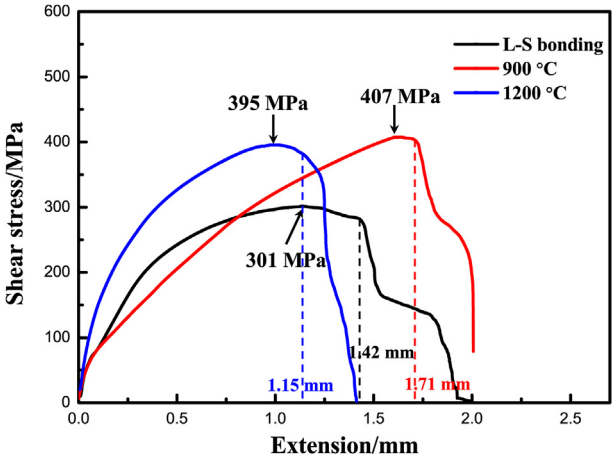

Fig. 4 – Shear stress–extension curves of the cladding interface of SS/CS laminated composite with different processing parameters.

for comparison of heterogeneous microstructures and their influences on the strength and ductility of the cladding interface. Finally, the strengthening mechanism of the heterogeneous lamella structure at the cladding interface zone were discussed.

2. Experimental methods

2.1. Liquid-solid bonding and hot rolling experiments

The 304 SS and Q235 CS were selected as the cladding material and substrate material, respectively. The chemical compositions were 0.074C–18.90Cr-9.10Ni-1.22Mn-0.089Si for the 304 SS and 0.18C-1.89Mn-0.044Si for the Q235 CS. The schematic diagram of preparing SS/CS laminated composite by L-S bonding method and the L-S bonded SS/CS laminated composite are shown in Fig. 1. The equipment mainly consists of a melting crucible and a compound casting mold, those were connected by a flow channel. The mold had an internal cavity section size of 58 mm × 33 mm, and was covered with high purity graphite. The polished Q235 CS plate with transverse dimensions of 50 mm × 25 mm was fixed in the center of the mold, then the mold was preheated by the induction coils. At the same time, the 304 SS was smelted in the crucible and kept at 1550 °C for 30 min, the melting temperature of the Q235 carbon steel is 1448 °C calculated using JMatPro software based on its compositions. In the meantime, the mold was preheated to 1400 °C and kept the temperature constant. After that, the 304 SS melt flowed into the mold through the flow channel, then turn off the induction coils and the SS/CS laminated composite with cladding layer thickness of 4 mm was cooled naturally in the mold. Finally, a L-S bonded SS/CS laminated composite with size of 100 mm × 57 mm x 33 mm was fabricated and cut into sizes of 100 mm × 11 mm × 16.5 mm, as shown in Fig. 1. The samples were heated at 900 °C or 1200 °C for 1 h and then hot rolled by multipass hot rolling with accumulated reduction rate of 50%. The reduction rates of hot rolling were 10%–20% per pass, and the hot rolled samples were reheated at an initial heating temperature for 3–5 min every two passes. The finishing rolling temperature of SS/CS laminated composites were controlled within the range of 850–1000 °C, and they were cooled naturally.

2.2. Microstructures and mechanical properties

The SS/CS laminated composite samples were prepared using standard metallographic techniques and etched by using solution of 5 g $CuSO_4$ + 100 ml HCl+100 ml C_2H_6O and 4% nitric acid alcohol for 304 SS and Q235 CS, respectively. Optical microscope (OM, OLYMPUS-BX53M) was used to characterize the microstructure of the samples. Electron probe microanalysis (EPMA, 1720H) was applied for analyzing the elemental distribution across the cladding interface of SS/CS laminated composite. The samples for EBSD were ground, mechanically polished and then vibration polished for 8–10 s, and were measured by using an EBSD detector (NordlysMax3) that installed in the TESCAN MIRA3 type SEM. In the observation of EBSD, an acceleration voltage of 20 kV, working distance of 15 mm and 2 μm step size were used. The hardness of the samples was measured using a HV-100 Vicker's indentation test machine with an applied load of 10 g and loading time of 10 s. The tensile shear test was conducted on an MTS810 universal testing machine with a strain rate of $1.0 \times 10^{-3}s^{-1}$, and dimensions of the tensile shear specimen is shown in Fig. 2.

3. Results

3.1. Mechanical properties of the cladding interface zone

Fig. 3 shows the relationship between the microhardness and the distance from the cladding interface. The 0 position on the x-coordinate represents the cladding interface, the left side is 304 SS and the right side is Q235 CS. It indicates that the peak value of microhardness appeared at the cladding interface, and sharply decreased toward two sides near the interface. In the 304 SS side, the microhardness gradually decreased and tended to be stable. However, the microhardness first reached valley bottom then increased and tended to be stable in the Q235 CS side. The average microhardness of 304 SS was higher than that of Q235 CS. Except the cladding interface, the microhardness of 304 SS and Q235 CS in L&R bonded SS/CS laminated composites were both higher than that in the L-S bonded SS/CS laminated composites. Additionally, the microhardness at the cladding interface and 304 SS hot rolled at 900 °C was obviously higher than that of hot rolled at 1200 °C. The microhardness of Q235 CS hot rolled at 900 °C was higher than that of hot rolled at 1200 °C within the range of 0–150 μm and greater than 1000 μm, while it was smaller within the range of 150–1000 μm.

The interfacial shear strength of the SS/CS laminated composites was measured by tensile shear test, and the relationship between the shear stress and extension is shown in Fig. 4. The interfacial shear strength of the L-S bonded SS/CS laminated composite was 301 MPa, indicating that a metallurgical bonding interface was obtained by L-S bonding method. The interfacial shear strength was significantly improved after hot rolling, and the maximum value of 407 MPa was obtained at rolling temperature of 900 °C, which was 35%

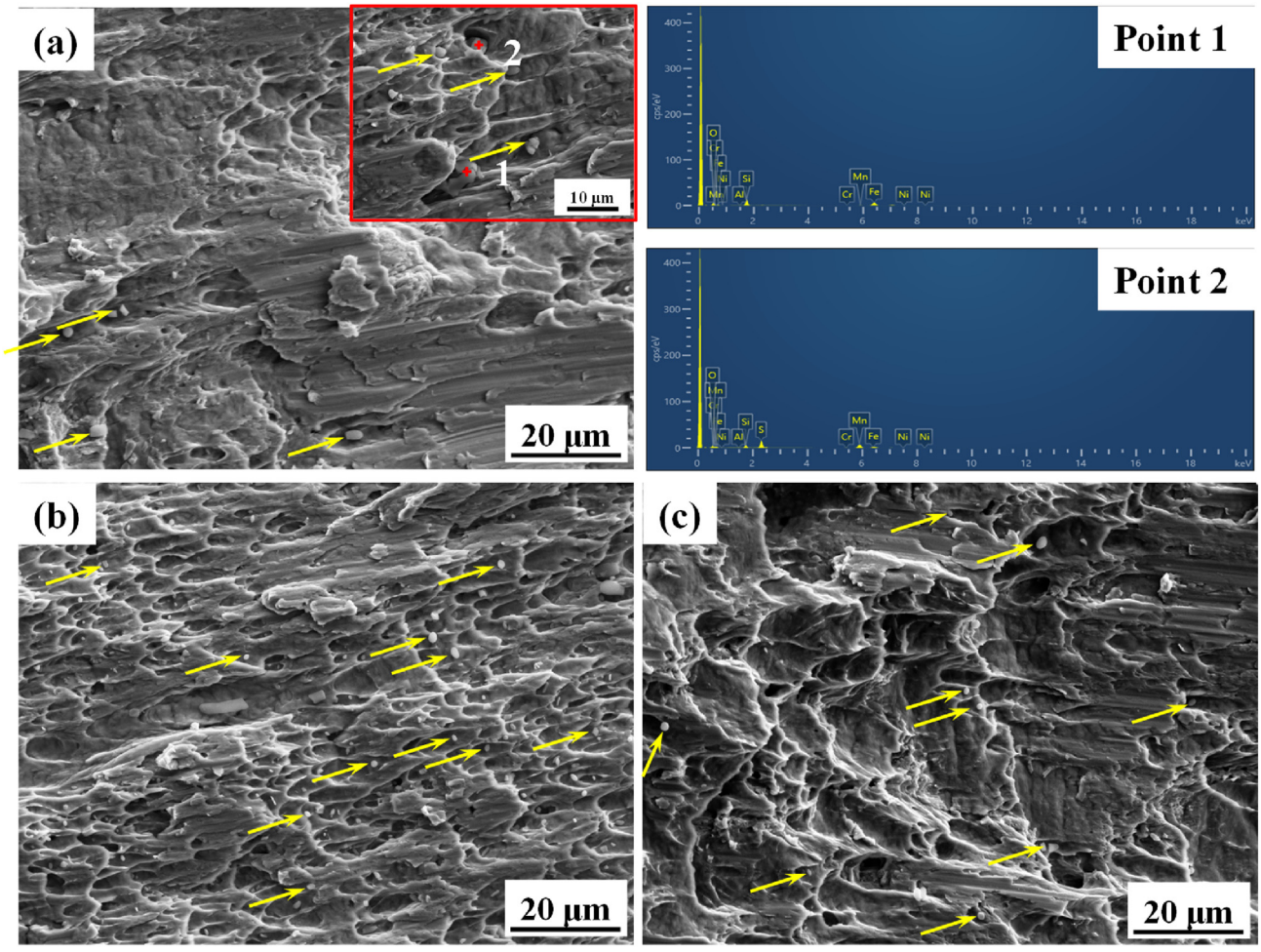

Fig. 5 – Tensile shear fracture morphologies of the SS/CS laminated composite with different processing parameters. (a) L-S bonding, L&R bonding with rolling temperatures of (b) 900 °C and (c) 1200 °C.

higher than that of the L-S bonded SS/CS laminated composite. The variation of shear stress can be divided into three stages as the extension increased, as displayed in Fig. 4. At the first stage, the shear stress increased linearly with increasing extension, indicating elastic deformation occurred at the cladding interface zone. The shear stress after elastic deformation were 41.4 MPa (L-S bonded), 35.6 MPa (hot rolled at 900 °C) and 74.5 MPa (hot rolled at 1200 °C) for the SS/CS laminated composites fabricated under different conditions. In the second stage, the shear stress increased while the increasing rate gradually decreased, indicating plastic deformation happened at the cladding interface zone. In the third stage, the shear strength fell abruptly after reaching the peak value, indicating fracture of the cladding interface zone. The shear stress–extension curves show that the SS/CS laminated composite hot rolled at 1200 °C had maximum shear stress after elastic deformation and minimum extension at fracture. Additionally, the SS/CS laminated composite hot rolled at 900 °C had minimum shear stress after elastic deformation and maximum extension of 1.71 mm at fracture.

The tensile shear fracture morphologies of the SS/CS laminated composites are shown in Fig. 5. The fracture morphologies of the L-S bonded SS/CS laminated composite presented few dimples and large cleavage surface, and there were white particles in the dimples. The EDS analysis of the particles indicated that they were Mn–Si–O inclusions and Mn–Si–O–S hybrid inclusions, as displayed in Fig. 5(a).

During the L-S bonding process, the Fe–O oxides on the surface of Q235 CS floated into the 304 SS melt, and then transformed into Cr–Mn–Si oxides during the subsequent cooling and solidification process. Additionally, MnS usually precipitates on the oxide surface and eventually forms the Mn–Si–O–S hybrid inclusions [47]. The quantities of dimples in the fracture of the L&R bonded SS/CS laminated composite increased after hot rolling, and the dimples size of SS/CS laminated composite hot rolled at 900 °C were much smaller than that of hot rolled at 1200 °C. Additionally, the quantity of inclusions indicated by yellow arrows increased after hot rolling and reached the maximum at rolling temperature of 900 °C. During the hot rolling process, the inclusions at the cladding interface were broken and squeezed into refined particles, and uniformly distributes at the cladding interface zone, which is beneficial to improve the interfacial bonding strength and toughness [15]. Lower rolling temperature induced higher stress during hot rolling process, resulting in stronger broken ability and increased quantities of inclusions.

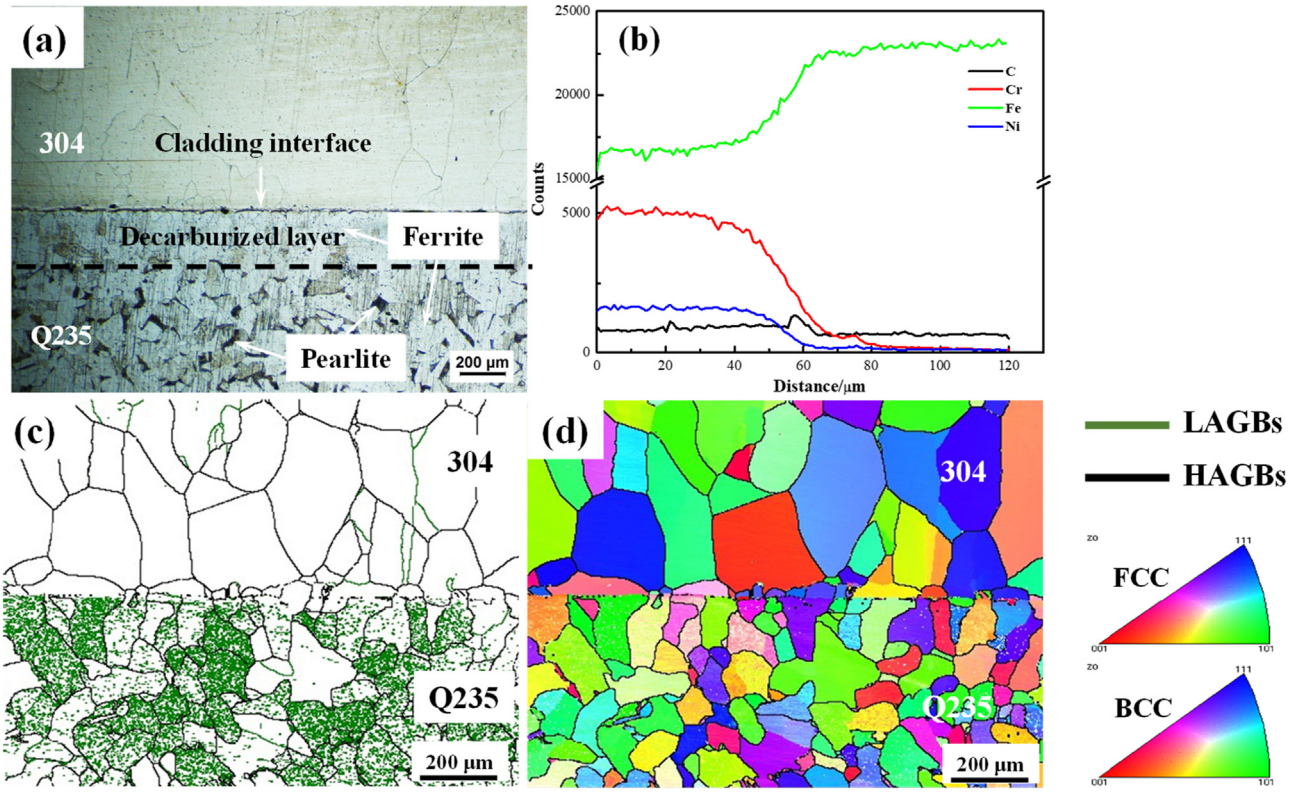

Fig. 6 – Microstructure characteristics at cladding interface zone of the liquid–solid bonded SS/CS laminated composite (a) OM micrograph, (b) compositions distribution through the cladding interface, (c) grain boundary map and (d) IPF map of Z-plane.

3.2. *Microstructures at the cladding interface zone of L-S bonded SS/CS laminated composite*

The microstructures at the cladding interface zone of L-S bonded SS/CS laminated composite were analyzed by OM, EPMA and EBSD, and the results are shown in Fig. 6. The equiaxed grains formed in both 304 SS and Q235 CS, and a decarburized layer of ferritic (thickness of 212 μm) formed in Q235 CS near the cladding interface, as displayed in Fig. 6(a). Fig. 6(b) shows the elements distribution across the cladding interface, the C element concentrated at the cladding interface and was less in the decarburized layer, while it gradually decreased as moving away from the cladding interface in the 304 SS. During the process of L-S bonding and hot rolling, C element diffused from the CS to SS due to chemical potential gradient, which results in the formation of decarburized layer and carburized layer in CS side and SS side, respectively. The variation of counts of C element in Fig. 6(b) indicated that the

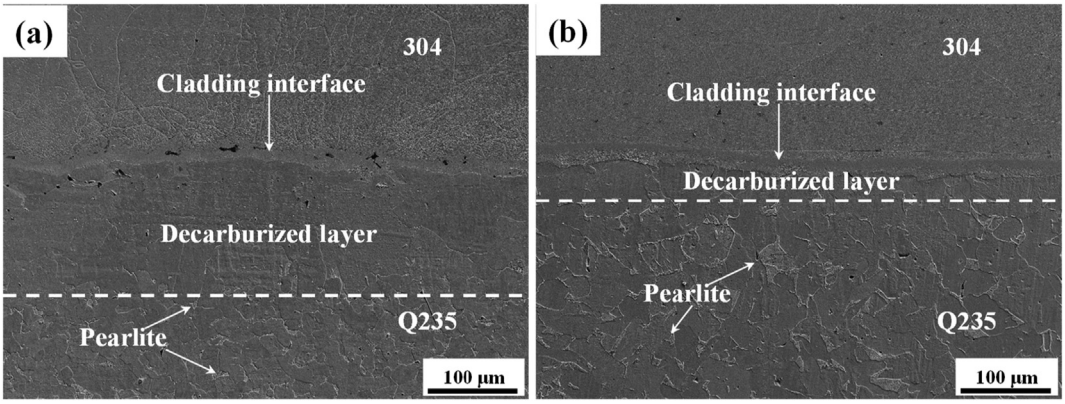

Fig. 7 – Microstructure at the cladding interface zone of L&R bonded SS/CS laminated composite with different rolling temperatures of (a) 900 °C and (b) 1200 °C.

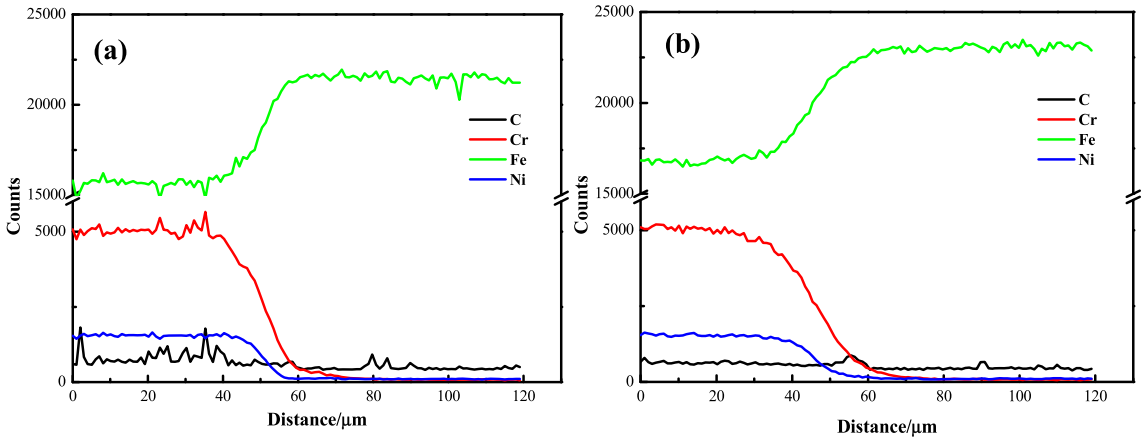

Fig. 8 – Distribution of C, Cr, Fe and Ni at the cladding interface zone of L&R bonded SS/CS laminated composite with different rolling temperatures of (a) 900 °C and (b) 1200 °C.

value fallen back nearly the nominal content of the SS at 40 μm from the cladding interface. Additionally, the diffusion distance of Cr, Ni and Fe elements were 64.5 μm, 35.0 μm and 39.2 μm, respectively. The distribution of grain boundaries is displayed in Fig. 6(c), the high angle grain boundaries (HAGBs) in black line were defined as the misorientation greater than 15°, while the low angle grain boundaries (LAGBs) in green line were defined as the misorientation within the range of 2°–15°. There were mainly HAGBs in the 304 SS while some retained LAGBs in the Q235 CS. During the L-S bonding process, the 304 SS melt solidified at the surface of Q235 CS and smaller grains appeared near the cladding interface due to higher cooling rate at the beginning. At the same time, intensive heat flux from 304 SS melt to Q235 CS substrate, leading to decreased cooling rate of 304 SS and increased temperature of Q235 CS. The Z-plane inverse pole figure (IPF) maps in Fig. 6(d) indicated randomly distributed grain orientations in both 304 SS and Q235 CS.

3.3. *Microstructure characteristics at the cladding interface zone of the L&R bonded SS/CS laminated composite*

The microstructures at the cladding interface zone of the L&R bonded SS/CS laminated composite were analyzed by SEM, and the results are shown in Fig. 7. It indicates that the decarburized layer still existed at the cladding interface zone, and the thickness of decarburized layer was 159 μm and 39 μm at hot rolling temperatures of 900 °C and 1200 °C, respectively. The thickness of decarburized layer decreased with increasing rolling temperature.

Fig. 8 shows the distribution of Cr, Ni, Fe and C elements across the cladding interface. The variation of Cr, Ni and Fe elements indicated three regions appeared at the cladding interface zone, those were 304 SS, compositional transition zone and Q235 CS, and the Cr, Ni and Fe content in the compositional transition zone emerged in gradient distribution. For the L&R bonded SS/CS laminated composites, there are fluctuations of C content appeared in both of 304 SS and Q235 CS, which results from the accumulation of C element and formation of carbides [15].

The interdiffusion of Cr, Ni and Fe elements across the cladding interface could dissolve in the matrix, which is beneficial to the interfacial bonding strength of the SS/CS laminated composites [16]. Further, the diffusion distances of Cr, Ni and Fe elements in the composition transition zone were statistically analyzed, and the results were shown in Table 1. It can be found that the diffusion distance of Cr was the largest, followed by that of Fe, and that of Ni was the smallest. The average diffusion distances of Cr, Fe and Ni elements decreased after hot rolling and increased with increasing hot rolling temperature. The L-S bonded SS/CS laminated composites were heated for 1 h before rolling, resulting in an increase of diffusion distance of Cr, Fe and Ni elements. Additionally, thermally activated atom jumping and external force induced atom jumping are two mechanisms for atomic diffusion in the process of hot rolling [48,49]. However, the width of the composition transition zone decreased as the extension along the rolling direction during hot rolling.

Table 1 – Diffusion distance of Cr, Fe and Ni at the cladding interface zone of L&R bonded SS/CS laminated composite with different rolling temperatures.

Diffusion distance/μm	900 °C	1200 °C
d_{Cr}	39.2	62.0
d_{Ni}	16.9	31.0
d_{Fe}	27.1	44.1

Table 2 – Microstructures characteristics of SS/CS laminated composite with different processing parameters.

Averaged grain size/μm	L-S bonding	L&R	
		900 °C	1200 °C
304 SS layer	110	65	39
Q235 CS layer	51	16	23
Coarse grained region	–	40	–
Fine grained region	–	15	–

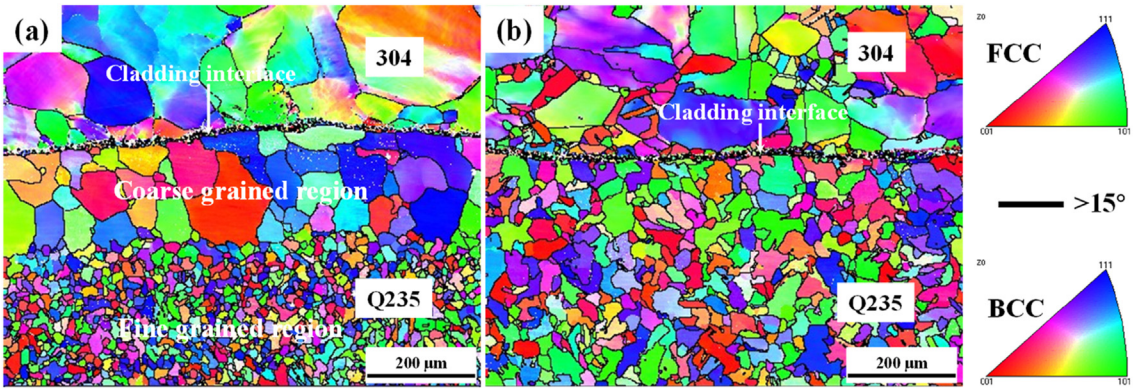

Fig. 9 – IPF map (Z-plane) of the L&R bonded SS/CS laminated composite under different rolling temperatures of (a) 900 °C and (b) 1200 °C.

The IPF maps of the L&R bonded SS/CS laminated composites are shown in Fig. 9, there were no preferred orientation but obvious difference in grain size distribution. At rolling temperature of 900 °C, there were two lamellated regions containing different grain sizes appeared in the Q235 CS side near the cladding interface. The region adjacent to the cladding interface contained coarse-grains, and the width of this region was about 185 μm. However, the region far away from the cladding interface contained fine-grains. However, the grain size was uniform in the Q235 CS at rolling temperature of 1200 °C. The grain size was measured according to the EBSD results and the average grain sizes are shown in Table 2. For the L-S bonded SS/CS laminated composite, the average grain size of 304 SS was 110 μm and the average grain size of Q235 CS was 51 μm. However, it indicates that the average grain size of 304 SS and Q235 CS all decreased after hot rolling. As shown in Fig. 9(a), the average grain size in coarse-grained region was 40 μm, while it was 15 μm in fine-grained region. At higher rolling temperature, the average grain size of 304 SS decreased while the average grain size of Q235 CS increased.

4. Discussion and analysis

4.1. *Formation mechanism of the heterogenous lamella structure*

As shown in Fig. 6, the deformed grains in Q235 CS recrystallized and grew up during L-S bonding process. Additionally, the 304 SS melt solidified on the surface of Q235 CS, and undistorted coarse grains formed due to lower cooling rate. The differences in composition, gain size and mechanical properties of the cladding interface zone in the L-S bonded SS/CS laminated composite strongly affected the deformation behavior and microstructure evolution during subsequent hot rolling process. Based on the EBSD observation, the misorientation angle of grains at the cladding interface zone of L&R bonded SS/CS laminated composites were obtained. According to the misorientation angle of grains, recrystallized grains were defined as having a misorientation angle less than 1°, deformed grains were defined as having a misorientation angle more than 7.5°, and grains with misorientation angles between 1° and 7.5° were defined as having a restored substructure. Fig. 10 displays the recrystallization characteristics at the cladding interface zone. As presented in Fig. 10(a), the 304 SS mainly contained deformed and restored substructures, while few fine recrystallized grains appeared near the HAGBs. Additionally, there were mainly restored substructures in the coarse-grained region while recrystallized grains in the fine-grained region of the Q235 CS. During hot rolling process, the decarburized layer had lower deformation activation energy comparing to adjacent regions, where plastic deformation first occurred in this region. The heterodeformation between the decarburized layer and adjacent regions induced strain gradient at the boundaries during plastic deformation, resulting in back stress strengthening and hardening of the decarburized layer. As a consequence, more strain occurred in the Q235 CS out of the decarburized layer, resulting in higher volume fraction of DRX and finer grains. However, the strengthened decarburized layer could not provide sufficient driving force of DRX under lower rolling temperature, resulting in lower volume fraction of DRX and coarse-grains. The width of the coarse-grained region was 187 μm and was nearly the width of decarburized layer. At rolling temperature of 1200 °C, the volume fraction of recrystallized grains increased and the gain size decreased in the 304 SS. However, uniform grains distributed in the Q235 CS and the coarse-grained region disappeared under this condition, which results from the decreased critical strain and increased driving force of DRX at higher rolling temperature. The EBSD results indicate that the volume fraction of the recrystallization and substructure in the 304 SS increased with increasing rolling temperature, as displayed in Fig. 10(c). The volume fraction of the recrystallization increased while the substructure and deformed grains decreased in the Q235 CS, as shown in Fig. 10(d).

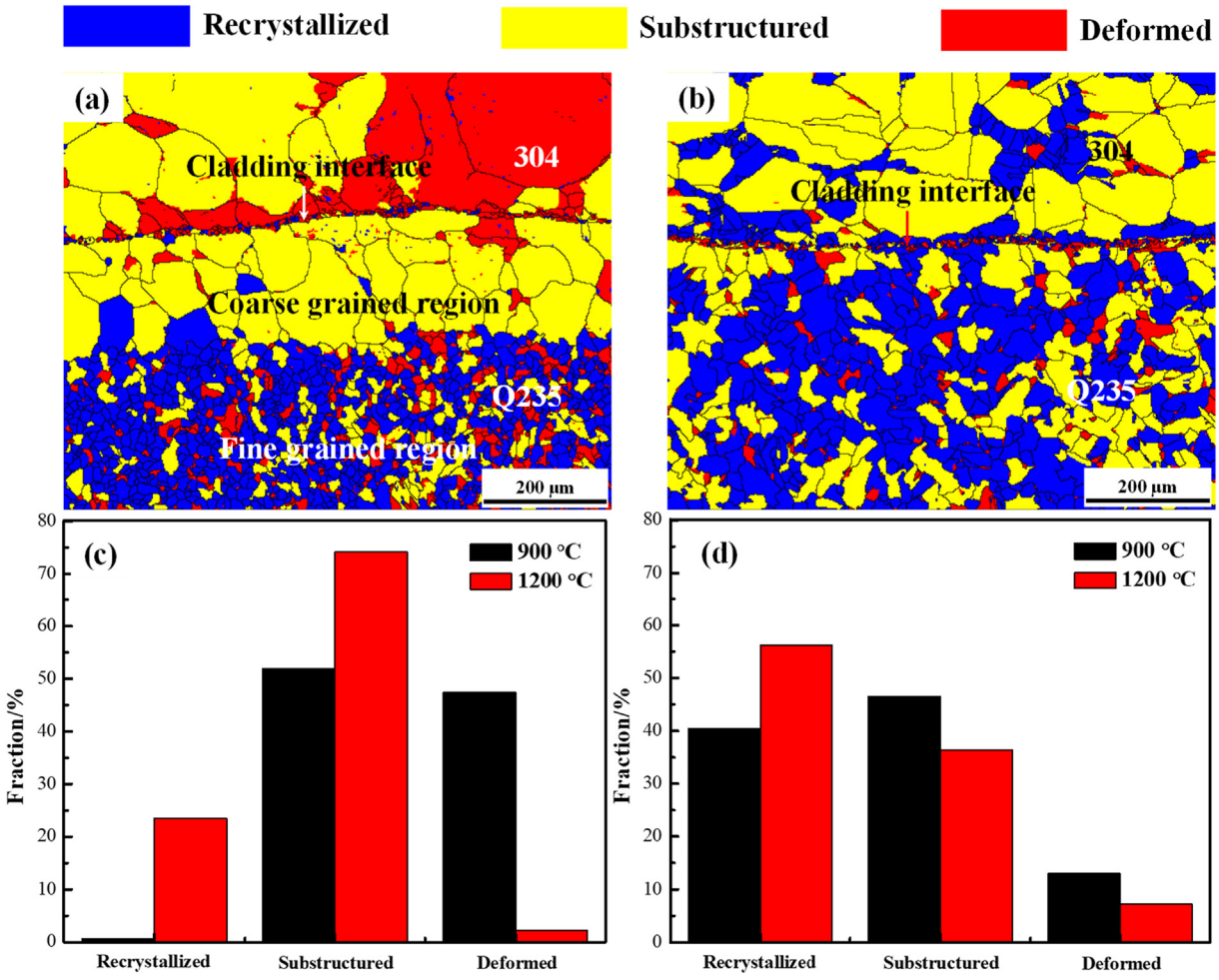

Fig. 10 – Recrystallization at the cladding interface zone of L&R bonded SS/CS laminated composite with different hot rolling temperatures of (a) 900 °C and (b) 1200 °C, volume fraction in (e) SS and (f) CS.

4.2. *Strengthening mechanism of the cladding interface*

Based on the EBSD results, the kernel average misorientation method can be used to calculate the local misorientation of the grains, and then the density of GNDs can be estimated according to Eq. (1) below.

$$\rho_{GND} = 2\theta/lb \tag{1}$$

where ρ_{GND} is the GNDs density at local points, θ is the misorientation at local points, l is the unit length for the local points (step size of EBSD was adopted in this study), b is the Burger's vector for the materials (the 304 SS is 0.253 nm, the Q235 CS is 0.248 nm) [50].

The distributions of GNDs density at the cladding interface zone of SS/CS laminated composites are shown in Fig. 11. As displayed in Fig. 11(a), the average GNDs density of 304 SS was 0.12×10^{14} m^{-2} and that of Q235 CS was 0.57×10^{14} m^{-2}. Lower cooling rate of 304 SS resulted in undistorted grains with lower GNDs density, and the recrystallization decreased the GNDs density of deformed Q235 CS. In the process of hot rolling, work hardening, dynamic recovery (DRV) and DRX occurred in the 304 SS and Q235 CS with the increase of strain. The work hardening led to the increase of GNDs density, while the DRV and DRX resulted in the decrease of GNDs density. The dynamic competition between work hardening and DRV and DRX determined the final GNDs density at the cladding interface zone. As shown in Fig. 11(b) and (c), the GNDs density increased significantly in the 304 SS side after hot rolling, and was higher at the cladding interface and HAGBs of 304 SS at hot rolling temperature of 900 °C. However, the GNDs density at the cladding interface and HAGBs of 304 SS decreased as the rolling temperature increased to 1200 °C, which results from higher driving force of DRV and DRX at higher temperature.

The domains of the cladding interface zone in Fig. 11 were uniformly divided into 20 regions paralleling to the cladding interface, and the average GNDs density of each region was calculated. The variations of average GNDs density versus the equivalent distance from the cladding interface were shown in Fig. 12. The 0 position on the x-coordinate represents the cladding interface, and the left side is 304 SS and the right side is Q235 CS. It can be found that the maximum value of GNDs density of the L-S bonded SS/CS laminated composite located in Q235 CS side near the cladding interface, and the GNDs density was much higher in Q235 CS than that in 304 SS. However, the peak value of GNDs density of L&R bonded SS/CS laminated

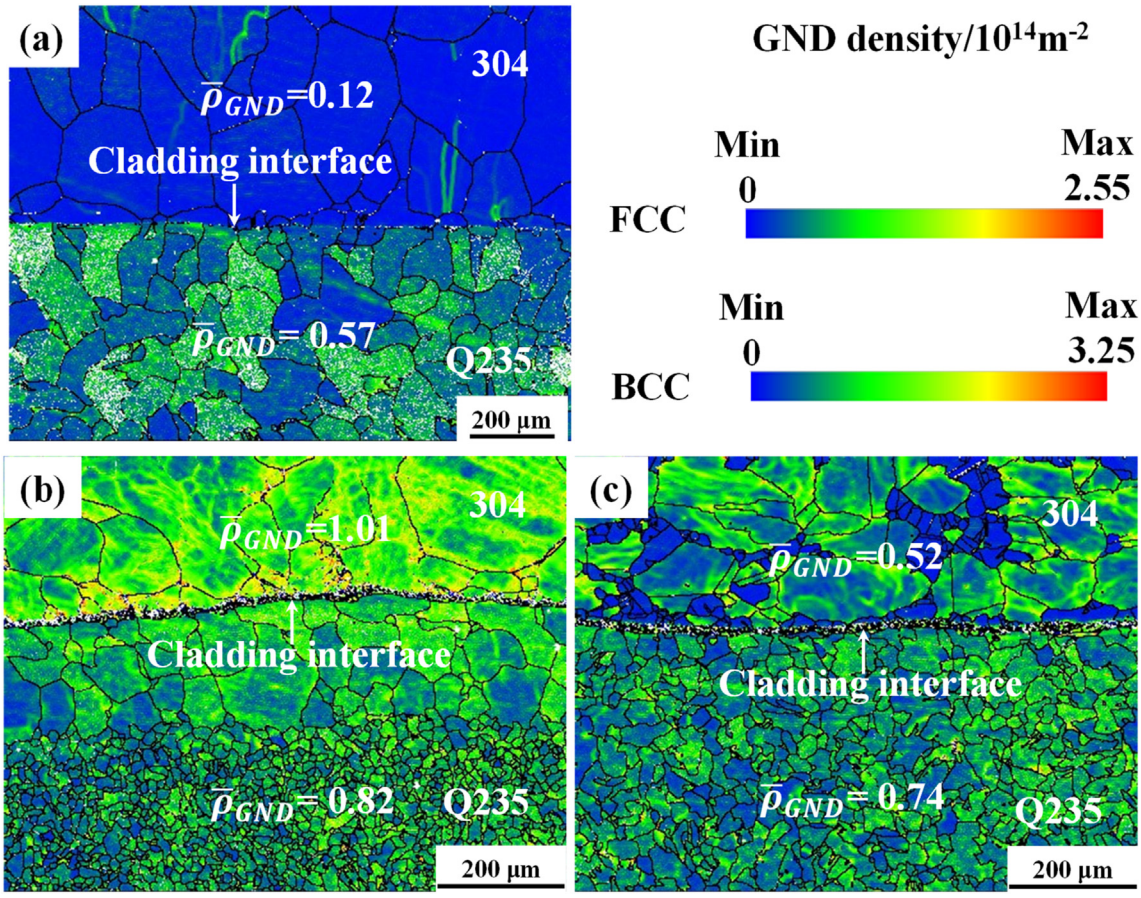

Fig. 11 – GNDs density maps of the cladding interface of SS/CS laminated composite with different processing parameters (a) L-S bonding, L&R bonding with rolling temperatures of (b) 900 °C and (c) 1200 °C.

composites appeared at the cladding interface, and then decreased to both sides and gradually tended to be stable, the average GNDs density increased in both 304 SS and Q235 CS after hot rolling. In the process of hot rolling, a strain gradient gradually formed at the cladding interface as deformation proceeding due to the mechanical incompatibility of austenite and ferrite, resulting in the pile-up of GNDs near the cladding interface. Additionally, the mechanical incompatibility of decarburized layer and Q235 CS substrate could also induce strain gradient at the boundary. Then the back stress was induced in decarburized layer to offset the applied stress for hindering dislocation emission and slip, leading to the strengthening and hardening of decarburized layer. Additionally, a forward stress was induced in the 304 SS and Q235 CS substrate outside the decarburized layer, which promotes plastic deformation and increases GNDs density there. With the increase of strain, GNDs density in Q235 CS and 304 SS increased, resulting in a significant strain hardening. However, the GNDs density in Q235 CS was much smaller than that in 304 SS due to higher volume fraction of DRX. For the L&R bonded SS/CS laminated composites, the GNDs density in 304 SS hot rolled at 900 °C was much higher than that hot rolled at 1200 °C due to lower recrystallization and higher work hardening during deformation, resulting in hardened austenite region near the cladding interface. Furthermore, higher strain hardening rate under lower deformation temperature of 900 °C induced higher GNDs density, and a GNDs density gradient formed at the boundary of coarse-grained region and fine-grained region due to mechanical incompatibility. When the rolling temperature was 1200 °C, higher driving force of DRX promoted the recrystallization in

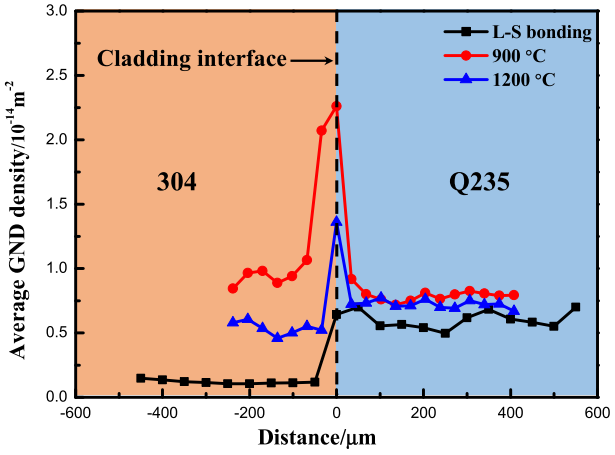

Fig. 12 – Variation of average GNDs density versus the equivalent distance from the cladding interface of SS/CS laminated composite with different processing parameters.

Table 3 – Difference of GNDs density of SS/CS laminated composite with different processing parameters.

GND density/$10^{14}m^{-2}$	L-S bonding	900 °C	1200 °C
ρ_{Q235}-ρ_{304}	0.44	−0.19	0.22
$\rho_{Interface}$-ρ_{304}	0.58	1.25	0.85
$\rho_{Interface}$-ρ_{Q235}	0.13	1.44	0.62
Average	0.36	1.35	0.74

the decarburized layer, resulting in the disappearance of the coarse-grained region and the decrease of GNDs density.

Table 3 shows the difference of average GNDs density between 304 SS and Q235 CS, and between the cladding interface and 304 SS or Q235 CS, respectively. It was found that higher difference of average GNDs density between cladding interface and the 304 SS or Q235 CS appeared in the L&R bonded SS/CS laminated composites hot rolled at 900 °C, while the average GNDs density in 304 SS was higher than that in Q235 CS. However, the average GNDs density in 304 SS was lower than that in Q235 CS of the L-S bonded SS/CS laminated composite and hot rolled at 1200 °C. It was reported that the difference of average GNDs density between the cladding and substrate layer gradually decreased with increasing strain, and reached the minimum value when the interface cracked [50]. Therefore, the heterogenous lamella structure of L&R bonded SS/CS laminated composites hot rolled at 900 °C induced stronger strengthening and hardening during plastic deformation, obviously improving the shear strength and ductility of the cladding interface.

As discussed above, a heterogenous lamella structure consisted of hardened austenite region, coarse-grained ferrite region and fine-grained pearlite and ferrite region formed at the cladding interface zone of L&R bonded SS/CS laminated composite under rolling temperature of 900 °C. Comparing with diffusion bonding and hot rolling bonding methods, a typical microstructure at the cladding interface zone of SS/CS laminated composites usually consists of recrystallized soften austenite region, ferrite region and pearlite and ferrite region with similar grain size, and the interfacial shear strength of the diffusion bonded and hot rolled SS/CS laminated composites under similar temperature or reduction rate are much smaller than that of L&R bonded SS/CS laminated composites with heterogenous lamella structure [10,12].

According to deformation physics of heterogeneous materials [51], the 304 SS and the Q235 CS both deform elastically with a small strain, and then the soft domains of the coarse-grained ferrite region started dislocation slip first to produce plastic strain. However, the hard domains of hardened austenite region and fine-grained pearlite and ferrite region remained elastic, which induces a plastic strain gradient in the coarse-grained ferrite region near the domain boundaries. In order to accommodate the strain gradient, numerous GNDs piled up at the boundaries, leading to the formation of a strong back stress in the coarse-grained ferrite region and restricting the slipping of dislocations, which made the coarse-grained ferrite region almost as strong as the hardened austenite region and fine-grained pearlite and ferrite region. Finally, these regions deformed both plastically as a co-deformation stage. Additionally, larger microhardness difference of the heterostructured cladding interface could induce stronger back stress during the elasto–plastic transition stage [50]. As a consequence, the combination of high strength and ductility could be obtained by heterogeneous lamella structure attributed to the back-stress hardening and strengthening induced by the strain gradient and pile-up of GNDs at the cladding interface zone with different mechanical properties [18,52].

5. Conclusions

(1) A new strategy of L-S bonding and subsequent hot rolling was proposed for fabricating SS/CS laminated composite, and the interfacial shear strength and extension of the L&R bonded SS/CS laminated composite reached the maximum of 407 MPa and 1.71 mm at rolled temperature of 900 °C.
(2) A metallurgical bonding interface with intensive elements diffusion was obtained by L-S bonding method, and a heterogenous structure containing coarse-grained region nearing the cladding interface and fine-grained region formed in the Q235 CS under hot rolling temperature of 900 °C.
(3) The mechanical incompatibilities of decarburized layer and coarse austenite results in the pile-up of GNDs near the cladding interface and a forward stress in the 304 SS, and promoted plastic deformation of austenite and increased GNDs density near the cladding interface and HAGBs, where recrystallization occurred firstly under higher rolling temperature.
(4) A heterogenous lamella structure consists of hardened austenite region, coarse-grained ferrite region and fine-grained pearlite region formed at the cladding interface zone of L&R bonded SS/CS laminated composite at rolling temperature of 900 °C, which obviously improves the interfacial shear strength and ductility of the SS/CS laminated composites.

Data availability

The processed data required to reproduce these findings cannot be shared at this time as the data also forms part of an ongoing study.

Declaration of Competing Interest

The authors declare that they have no known competing financial interests or personal relationships that could have appeared to influence the work reported in this paper.

Acknowledgement

This work was supported by the National Key R&D Program of China (No. 2018YFA0707300), the National Natural Science Foundation of China (No. 52004028, No. 51904029).

REFERENCES

[1] Dhib Z, Guermazi N, Ktari A, Gasperini M, Haddar N. Mechanical bonding properties and interfacial morphologies of austenitic stainless steel clad plates. Mater Sci Eng, A 2017;696:374–86.

[2] Xue JL, Bouchard J, Chen XD, Fan ZC, Zhou Y. Anisotropic elastic constants calculation of stainless steel cladded layers of pressure vessel steel plate. Int J Pres Ves Pip 2019;177:103991.

[3] Song H, Shin H, Shin Y. Heat-treatment of clad steel plate for application of hull structure. Ocean Eng 2016;122:278–87.

[4] Suzuki S, Muraoka R, Obinata T, Endo S, Horita T, Omata K. Steel products for shipbuilding. JFE Tech Rep 2004;(2):41–8.

[5] Rees DWA, Power RK. Forming limits in a clad steel. J Mater Process Technol 1994;45:571–5.

[6] Li HB, Chen J, Yang J. Experiment and numerical simulation on delamination during the laminated steel sheet forming processes. Int J Adv Manuf Technol 2013;68:641–9.

[7] Liu BX, Huang LJ, Rong XD, Geng L, Yin FX. Bending behaviors and fracture characteristics of laminated ductile-tough composites under different modes. Compos Sci Technol 2016;126:94–105.

[8] Meng YF, Kang K, Gao M, Zeng XY. Microstructures and properties of single-pass laser-arc hybrid welded stainless clad steel plate. J Manuf Process 2018;36:293–300.

[9] Kaya Y, Kahraman N. An investigation into the explosive welding/cladding of Grade A ship steel/AISI 316L austenitic stainless steel. Mater Des 2013;52:367–72.

[10] Li Q, Chen WF, Du JL, Lu MW, Wang ZM, Huang Y. Microstructure and coordination mechanism of interface of stainless steel/carbon steel cladding plate prepared by vacuum diffusion bonding. Mater Sci Eng, A 2022;829:142178.

[11] Zhu ZC, He Y, Zhang XJ, Liu HY, Li X. Effect of interface oxides on shear properties of hot-rolled stainless steel clad plate. Mater Sci Eng, A 2016;669:344–9.

[12] Jing YA, Qin Y, Zang XM, Li YH. The bonding properties and interfacial morphologies of clad plate prepared by multiple passes hot rolling in a protective atmosphere. J Mater Process Technol 2014;214(8):1686–95.

[13] Liu BX, Wang S, Fang W, Ma JL, Yin FX, Feng JN, et al. Microstructure and mechanical properties of hot rolled stainless steel clad plate by heat treatment. Mater Chem Phys 2018;216:460–7.

[14] Chen CX, Liu MY, Liu BX, Yin FX, Dong YC, Zhang X, et al. Tensile shear sample design and interfacial shear strength of stainless steel clad plate. Fusion Eng Des 2017;125:431–41.

[15] Liu BX, Yin FX, Dai XL, He JN, Fang W, Chen CX, et al. The tensile behaviors and fracture characteristics of stainless steel clad plates with different interfacial status. Mater Sci Eng, A 2017;679:172–82.

[16] Liu BX, Wang S, Chen CX, Fang W, Feng JH, Zhang X, et al. Interface characteristics and fracture behavior of hot rolled stainless steel clad plates with different vacuum degrees. Appl Surf Sci 2019;463:121–31.

[17] Lu K. Making strong nanomaterial ductile with gradients. Science 2014;345:1455–6.

[18] Wu XL, Yang MX, Yuan FP, Wu GL, Wei YJ, Huang XX, et al. Heterogeneous lamella structure unites ultrafine-grain strength with coarse-grain ductility. Proc Natl Acad Sci USA 2015;112:14501–5.

[19] Ma XL, Huang CX, Moering J, Ruppert M, Hoppel HW, Goken M, et al. Mechanical properties in copper/bronze laminates: role of interfaces. Acta Mater 2016;116:43–52.

[20] Ma E, Zhu T. Towards strength-ductility synergy through the design of heterogeneous nanostructures in metals. Mater Today 2017;20(6):323–31.

[21] Ding H, Cui XP, Wang ZQ, Zhao T, Wang YC, Zhang YY, et al. A new strategy for fabrication of unique heterostructured titanium laminates and visually tracking their synchronous evolution of strain partitions versus microstructure. J Mater Sci Technol 2022;107:70–81.

[22] Lee S-B, LeDonne JE, Lim SCV, Beyerlein IJ, Rollett AD. The heterophase interface character distribution of physical vapor-deposited and accumulative roll-bonded Cu-Nb multilayer composites. Acta Mater 2012;60:1747–61.

[23] Liu XC, Zhang HW, Lu K. Formation of nano-laminated structure in nickel by means of surface mechanical grinding treatment. Acta Mater 2015;96:24–36.

[24] Mishin Y, Asta M, Li J. Atomistic modeling of interfaces and their impact on microstructure and properties. Acta Mater 2010;58:1117–51.

[25] Yang DK, Cizek P, Fabijanic D, Wang JT, Hodgson PD. Work hardening in ultrafine-grained titanium: multilayering and grading. Acta Mater 2013;61:2840–52.

[26] Zhang J, Wang XH, Wang WJ, Zhang LJ, Xu ZB. Investigation of microstructure and interface shear strength of austenitic stainless steel composite strip produced with inversion casting method. J Univ of Sci Technol Beijing 2000;22(2):113–6.

[27] Vidoni M, Ackermann R, Richter S, Hirt G. Production of clad steel strips by twin-roll strip casting. Adv Eng Mater 2015;17(11):1588–97.

[28] Chen G, Li JT, Xu GM. Bonding process and interfacial reaction in horizontal twin-roll casting of steel/aluminum clad sheet. J Mater Process Technol 2017;246:1–12.

[29] Yang Y, Laird BB. Droplet spreading on a surface exhibiting solid-liquid interfacial premelting. Acta Mater 2018;143:319–28.

[30] Sumita T, Kobayashi Y. Dissolution behavior of solid stainless steel by its molten eutectic mixture with B_4C under dynamic condition. Prog Nucl Energy 2019;117:103094.

[31] Chakraborty P, Naveen Kumar N, Sai Krishna N, Maheshwari NK, Bysakh S, Bose A, et al. Effect of oxide layer and the duration of exposure on the liquid metal corrosion mechanism of RAFM steel in molten Pb-Li. Corrosion Sci 2021;183:109321.

[32] Xu C, Meng XC, Sun XG, Gan XL, Li P, Xiao SF, et al. Atomic scale analysis of the corrosion characteristics of Cu-Li solid-liquid interfaces. J Alloys Compd 2018;763:1–10.

[33] Huang HG, Ji C, Yang ZQ, Yan M. Implementation and forming mechanism of the solid-liquid cast-rolling bonding (SLCRB) process for steel/Al clad pipes. J Manuf Process 2017;30:343–52.

[34] Jia Q, Lai ZW, Zhang HQ, Bai HL, Zou GS, Pan C, et al. Mechanism of ultrasonic-assisted transient liquid phase bonding of 6061 Al alloy with cladded Zn-Al alloy in air. J Mater Process Technol 2020;286:116823.

[35] Kokabi D, Kaflou A, Gholamipour R, Pouranvari M. Microstructural evaluation during dissimilar transient liquid phase bonding of TiAl/Ni-based superalloy. J Alloys Compd 2020;825:153999.

[36] Bakke AO, Arnberg L, Løland J-O, Jørgensen S, Kvinge J. Formation and evolution of the interfacial structure in Al/steel compound castings during solidification and heat treatment. J Alloys Compd 2020;849:156685.

[37] Pierce DT, Field DM, Limmer KR, Muth T, Sebeck KM. Hot deformation behavior of an industrially cast large grained low density austenitic steel. Mater Sci Eng, A 2021;825:141785.

[38] Zhao HT, Qi JJ, Liu GQ, Su R, Sun ZH. A comparative study on hot deformation behaviours of low-carbon and medium-carbon vanadium microalloyed steels. J Mater Res Technol 2020;9(5):11319–31.

[39] Lan L, Zhou W, Misra RDK. Effect of hot deformation parameters on flow stress and microstructure in a low carbon microalloyed steel. Mater Sci Eng, A 2019;756:18–26.
[40] Wahabi ME, Gavard L, Montheillet F, Cabrera JM, Prado JM. Effect of initial grain size on dynamic recrystallization in high purity austenitic stainless steels. Acta Mater 2005;53(17):4605–12.
[41] Manshadi AD, Barnett MR, Hodgson PD. Recrystallization in AISI 304 austenitic stainless steel during and after hot deformation. Mater Sci Eng, A 2008;485(1–2):664–72.
[42] Miura H, Ozama M, Mogawa R, Sakai T. Strain-rate effect on dynamic recrystallization at grain boundary in Cu alloy bicrystal. Scripta Mater 2003;48(10):1501–5.
[43] Tabatabaee SE, Mousavi-Anijdan SH, Najafi H. Hot deformation mechanisms, mechanical properties and microstructural evolution of a HP-Nb steel. Mater Sci Eng, A 2020;800:140326.
[44] Rajput SK, Chaudhari GP, Nath SK. Characterization of hot deformation behavior of a low carbon steel using processing maps, constitutive equations and Zener-Hollomon parameter. Mater Sci Eng, A 2016;237:113–25.
[45] Liu ZY, Wang HZ, Hache MJR, Chu X, Irissou E, Zou Y. Characterization of hot deformation behavior of a low carbon steel using processing maps, constitutive equations and Zener-Hollomon parameter. Acta Mater 2020;193:191–201.
[46] Huang K, Logé RE. A review of dynamic recrystallization phenomena in metallic materials. Mater Des 2016;111:548–74.
[47] Ren Y, Zhang LF, Pistorius PC. Transformation of oxide inclusions in type 304 stainless steel during heat treatment. Metall Mater Trans B 2017;48B:2281–92.
[48] Martin G, Bellon P. Radiation effects in concentrated alloys and compounds: equilibrium and kinetics of driven systems. C. R. Physique 2008;9:323–34.
[49] Wang CY, Jiang YB, Xie JX, Zhou DJ, Zhang XJ. Interface formation and bonding mechanism of embedded aluminum-steel composite sheet during cold roll bonding. Mater Sci Eng, A 2017;708:50–9.
[50] He JY, Ma Y, Yan DS, Jiao SH, Yuan FP, Wu XL. Improving ductility by increasing fraction of interfacial zone in low C steel/304 SS laminates. Mater Sci Eng, A 2018;726:288–97.
[51] Yang MX, Yuan FP, Xie QG, Wang YD, Ma E, Wu XL. Strain hardening in Fe-16Mn-10Al-0.86C-5Ni high specific strength steel. Acta Mater 2016;109:213–22.
[52] Yuan R, Beyerlein IJ, Zhou CZ. Homogenization of plastic deformation in heterogeneous lamella structures. Mater. Res. Let. 2017;5:251–7.